Analysis of critical parameters for nonrelativistic models of symmetric nuclear matter

Mariana Dutra [],[1] Odilon Lourenço [],[1,*] Xavier Viñas,[2] and C. Mondal [][2,3]

[1]*Departamento de Física, Instituto Tecnológico de Aeronáutica, DCTA, 12228-900 São José dos Campos, São Paulo, Brazil*
[2]*Departament de Física Quàntica i Astrofísica and Institut de Ciències del Cosmos (ICCUB), Facultat de Física, Universitat de Barcelona, Martí i Franquès 1, E-08028 Barcelona, Spain*
[3]*LPC Caen, Université de Caen Normandie, F-14000 Caen, France*

In this work we have analyzed several features of symmetric nuclear matter (SNM) at finite temperature described by different zero- and finite-range nonrelativistic families of models, namely, Skyrme, Gogny, momentum-dependent interaction, Michigan three-range Yukawa, and simple effective interaction. We have calculated the critical parameters (CPs) associated to the liquid-gas phase coexistence for nuclear matter from these parametrizations and show that they are in agreement with their experimental and theoretical values obtained in the literature. Our study also points to a strong evidence of universality presented by the hadronic models, namely, model independence in the gaseous phase and distinguishability among different interactions in the liquid phase. We have performed a correlation study among different CPs and SNM properties. Such studies involving different finite-range interactions are scarce in literature. The analyzed models show an overall increasing trend of the critical temperature as a function of critical pressure.

I. INTRODUCTION

Hadronic models show very interesting features when they are used to describe warm nuclear matter at nonvanishing temperatures. Due to nucleon-nucleon interaction, thermodynamical liquid and gas phases coexist below a certain temperature, named the critical temperature, exhibiting a van der Waals pattern. The different thermodynamical quantities such as the pressure (P_c) or the density (ρ_c) at this junction point along with the temperature T_c are denoted together as critical parameters. The analysis of such phase structure can lead to a deeper understanding of the nuclear interaction in different environments such as heavy-ion collisions [1,2] and finite nuclei [3–5], for instance. In nonaccreting neutron stars, finite temperature calculations might also play some crucial roles to determine the structure and composition of their crusts [6,7]. Furthermore, a suitable knowledge of the hadronic equations of state at $T > 0$ is crucial to describe correctly different astrophysical phenomena such as core-collapse supernovas or neutron star mergers [8,9]. Correlation studies among the nuclear matter properties (at $T = 0$) and critical parameters ($T > 0$) also carry vital information regarding the nuclear equation of state and in turn the basic nature of the nucleon-nucleon interaction in medium [10]. In other words, if strong enough correlations are established between T_c, P_c, and ρ_c with the bulk parameters of hadronic models, any direct or indirect experimental constraints established in a particular set of these quantities might be useful to pin down the other ones.

Equations of state are obtained by using nuclear models of different degrees of sophistication. Explaining nuclear phenomena based on a theory starting from fundamental nucleon-nucleon interaction is yet to be achieved. The nonperturbative nature of the nuclear force makes it very difficult to be described starting from the strong interaction between quarks and gluons. Over the years, developing effective theories by optimizing few parameters fitted to certain experimental data has been a hallmark of the development of the nuclear theory. As an example, the ground state energy of a nucleus, which is defined as the negative of its binding energy $B(A, Z)$, was proposed a long time ago by Weizsäcker [11] in a model (semiempirical mass formula) that considers the nucleus as a droplet of incompressible matter with $B(A, Z)$ containing terms proportional to its volume, surface, etc. [12]. Many sophisticated models have been constructed since then, successfully describing different features of finite nuclei and infinite nuclear matter. Some of them, not necessarily in the chronological order of appearing, are described in the following.

In chiral effective field theory (EFT) models (see Ref. [13] and references therein), the most general Lagrangian density is proposed with the basic symmetries of quantum chromodynamics, in particular the chiral symmetry. The low-energy regime of this theory is obtained with the quarks confined into the colorless hadrons giving rise to the more suitable degrees of freedom for this energy scale [13]. However, nuclear forces based on chiral EFT also pose some major challenges to be applied in nuclear structure [14] and reactions (see Ref. [15] and references therein).

In its effective finite-range version, the relativistic mean-field (RMF) models explicitly describe the attractive and repulsive nuclear interactions by including in the Lagrangian

*odilon.ita@gmail.com

density the fermion field ψ coupled to the scalar and vector mesons fields σ and ω_μ, respectively. The structure of the model also generates scalar and vector potentials that largely cancel each other at a particular density, giving rise to a relativistic mechanism for the nuclear matter saturation. In its point-coupling version, the RMF models consider a zero-range interaction between the nucleons, and ψ is the only field in this case. For the finite-, zero-range, and even improved versions of this model, see Refs. [16–18]. The density-dependent meson exchange (DDME) version of the RMF models also describes several ground state finite nuclear properties satisfactorily [19].

The nonrelativistic Skyrme model considers nucleons interacting with each other through two- and three-body point-like interactions [20–24]. Its two-body potential is written as a contact term times a low-momentum expansion function, taken up to quadratic order in the momenta. The three-body interaction is given by the product of two delta functions, which can be also interpreted as a two-body density-dependent interaction. Different thermodynamical quantities in Skyrme models can be obtained in a relatively simple way [25], as they can be expressed as functions of the nuclear density and the proton fraction (zero-temperature regime). Such ease in implementation has made Skyrme models so popular over the years. It has also been successfully applied to finite nuclei reproducing with very good accuracy the ground state energies, giant resonances, and other physical properties [26].

The standard Gogny models of the D1 family consist of two finite-range terms of Gaussian type, which include all the possible spin-isospin exchange operators with different weights, plus a zero-range density-dependent contribution [27]. The main property of Gogny interaction is that it can describe simultaneously the mean field and the pairing field. The Gogny interactions correctly describe many features of finite nuclei, in particular their pairing and deformation properties, along the whole periodic table [28–30]. Although Gogny forces of the D1 family do not describe properly the properties of neutron stars [31,32], recent progress has been made in this direction [33,34].

The momentum-dependent interaction (MDI) was primarily designed to be used in heavy-ion collisions [35]. Similar to the Gogny forces, the MDI can be written as a single finite-range term of Yukawa type, along with two zero-range contributions. Although the first versions of the MDIs were adequate to describe collisions of symmetric nuclei, more recent versions of this force are able to describe collisions of neutron-rich nuclei at intermediate energies [18,36]. The MDI is constructed in such a way that it is possible to obtain a family of forces with the same properties of symmetric matter but with variation in the isovector sector of the force [18,36], which makes these interactions very appealing to be used in the calculations of neutron star properties [37].

The so-called Michigan three-range Yukawa (M3Y) models [38] were derived from a bare nucleon-nucleon interaction (Paris, Reid) by fitting the microscopic G-matrix to the sum of three Yukawa form factors of different ranges acting on the different spin-isospin states. It should be pointed out that the original M3Y force was unable to reproduce the saturation and spin-orbit splitting at mean-field level. To solve this problem,

zero-range terms were added and some strengths were modified [39]. The tensor force, which is important for describing the shell structure in finite nuclei, has been included in the different M3Y parametrizations [39–42]. To describe open-shell nuclei, pairing correlations have been taken into account using the M3Y force in the particle-particle channel together with a cutoff in momentum space [40]. It is also important to mention that the interactions of the M3Y type have been applied successfully to describe different nuclear reactions [43].

The simple effective interaction (SEI) was constructed in 1998 by Behera and collaborators [44] and aimed to describe nuclear and neutron star matter at zero and finite temperatures. The SEI consists of a single finite-range term with a form factor of Gauss or Yukawa type, a pure contact term, and a zero-range density-dependent contribution, which contains an additional parameter to avoid the supraluminous behavior at any temperature [44]. At variance with other effective interactions like Skyrme, Gogny, or M3Y type, 9 out of the 11 parameters of SEI are fitted to empirical constraints and microscopic results obtained with realistic interactions in nuclear matter. In this way SEI predicts the correct behavior of the momentum dependence of the mean field as extracted from heavy-ion collisions at intermediate energies. SEI also predicts trends of Dirac-Brueckner-Hartree-Fock and variational calculations in nuclear and neutron matter. One of the remaining two parameters is fixed from the microscopic spin-up–spin-down splitting of the effective mass in polarized neutron matter [45]. The last parameter, together with the strength of the spin-orbit contribution, is determined from Hartree-Fock calculations in finite nuclei [46,47]. It is worthwhile to point out that, in spite of the fact that almost all the parameters of SEI are determined in nuclear matter, its finite nuclei description has a quality similar to that found using successful effective interactions like Skyrme, Gogny, or M3Y.

In a previous investigation, we used RMF models to calculate different characteristics of nuclear matter at finite temperature [10]. In the present work, we intend to complement that study with calculations performed for different nonrelativistic models. To this end, we study the nonrelativistic Skyrme, Gogny, MDI, M3Y, and SEI models in the finite temperature regime in order to compute different critical parameters and compare them with experimental and theoretical results. We also investigate the connection between these quantities with some bulk parameters, namely, incompressibility and nucleon effective mass, both calculated for symmetric nuclear matter at zero temperature. In Sec. II we outline the main theoretical quantities regarding the nonrelativistic models studied in this work (expressions at finite temperature). The outcomes of the finite temperature calculations are shown in Sec. III, and in Sec. IV a short summary and our concluding remarks are presented.

II. NONRELATIVISTIC MODELS AT FINITE TEMPERATURE

A. Skyrme model

An advantage of the Skyrme model is that its point-like nucleon-nucleon interaction implies a Hamiltonian as a

function only of the nuclear density ρ for symmetric systems. In the mean-field approach, the single-particle state of the nucleon in a uniform medium is written in terms of a plane waves [48]. As a consequence, it is straightforward to construct, at zero temperature, the energy density of the system and therefore to derive all the other thermodynamical quantities needed to describe nuclear matter (see, for instance, Ref. [49] for such calculations).

In the finite temperature regime the Heaviside step function ($\theta(k_F - k)$ with k_F being the Fermi momentum in units of fm^{-1}), present in all the momentum integrals at zero temperature, is replaced by the Fermi-Dirac function (momentum distribution), depending on momentum k, temperature T, and an effective chemical potential μ, which is given by

$$n_{\text{sky}}(k) = \frac{1}{e^{[\varepsilon^*(k)-\mu]/T} + 1},\qquad(1)$$

where $\varepsilon^*(k) = \hbar^2 k^2 / 2M^*$ is the single-particle energy with M^* being the effective mass. As a consequence, for warm nuclear matter the nuclear density becomes [50,51]

$$\rho = \frac{\gamma}{(2\pi)^3} \int d\mathbf{k}\, n_{\text{sky}}(k),\qquad(2)$$

where γ is the degeneracy factor ($\gamma = 4$ for symmetric nuclear matter). For the Skyrme model, the nucleon effective mass in the single-particle energy ε^* is defined from the energy density as its variation with respect to the kinetic energy density. It is given by

$$M^* = M\left[1 + \frac{1}{8}\frac{M}{\hbar^2}\rho(3t_1 + 5t_2 + 4t_2 x_2)\right]^{-1},\qquad(3)$$

in which $M = 939$ MeV is the free nucleon mass. Notice that in Eq. (2) the momentum distribution depends on M^* instead of M. For the numerical calculations, the van der Waals–like isotherms are obtained for a fixed temperature and run over the density. For a particular ρ, we invert Eq. (2) in order to find the value of the chemical potential μ. Then, for each ρ we can compute the momentum distribution, which enters in all the other thermodynamical quantities, since the corresponding value of μ is determined. As we are interested in the critical parameters of the model, obtained through the following conditions,

$$P_c = P(\rho_c, T_c),\quad \left.\frac{\partial P}{\partial \rho}\right|_{\rho_c, T_c} = 0,\quad \left.\frac{\partial^2 P}{\partial \rho^2}\right|_{\rho_c, T_c} = 0,\qquad(4)$$

it is only needed to construct the pressure of the system, since it is the most relevant thermodynamical quantity for this purpose. For the Skyrme model it reads

$$P_{\text{sky}}(\rho, T) = \frac{3t_0}{8}\rho^2 + \frac{1}{16}\sum_{i=1}^{3} t_{3i}(\sigma_i + 1)\rho^{\sigma_i + 2}$$
$$+ \frac{\gamma\hbar^2}{6\pi^2 M^*}\left(1 - \frac{3}{2}\frac{\rho}{M^*}\frac{dM^*}{d\rho}\right)\int_0^\infty dk\, k^4 n_{\text{sky}}(k).\qquad(5)$$

For the symmetric system, a particular parametrization of the Skyrme model is defined by a specific set of the following free parameters: x_2, t_0 (MeV fm^3), t_1 (MeV fm^5), t_2 (MeV fm^5), t_{3i} (MeV fm$^{3(\sigma_i+1)}$), and σ_i. Here, we mainly focus on the consistent Skyrme parametrizations (CSkPs)

selected in Ref. [49]. In that work, the authors selected 16 Skyrme parametrizations that satisfy the 11 constraints coming from nuclear matter, pure neutron matter, analysis of symmetry energy, and its derivatives. They are GSkI [52], GSkII [52], KDE0v1 [53], LNS [54], MSL0 [55], NRAPR [56], Ska25s20 [57], Ska35s20 [57], SKRA [58], Skxs20 [59], SQMC650 [60], SQMC700 [60], SkT1 [61], SkT2 [61], SkT3 [61], and SV-sym32 [62]. Among these parametrizations, only two are "nonstandard," namely, GSkI and GSkII. The term nonstandard refers here to those parametrizations for which i is not equal to 1 in Eq. (5). In particular, GSkI and GSkII were shown to fit consistently the masses of some spherical nuclei, namely, ^{16}O, ^{24}O, ^{14}Ca, ^{48}Ca, ^{48}Ni, ^{56}Ni, ^{68}Ni, ^{78}Ni, ^{88}Sr, ^{90}Zr, ^{100}Sn, ^{132}Sn, and ^{208}Pb. The CSkP was also shown to be consistent [63] with the constraints extracted from the LIGO and Virgo Collaboration analysis, related to the detection of gravitational waves coming from the neutron star merger GW170817 event [64–66]. For the sake of completeness, we also add to our analysis four more Skyrme parametrizations. Three of them are constrained by chiral effective field theory [67], namely, Skχ414, Skχ450, and Skχ500, and another one is taken from Ref. [68], SkΛ267. For the last one, the dimensionless tidal deformability of the $1.4M_\odot$ neutron star is given by $\Lambda_{1.4} = 267$, with the corresponding radius of $R_{1.4} = 11.6$ km.

B. Finite-range interactions

The finite-range (FR) interactions that we study in this work, namely, Gogny, MDI, M3Y, and SEI, have a similar structure, which can be written as

$$V(\mathbf{r}_1, \mathbf{r}_2) = \sum_{i=1}^{N}(W_i + B_i P_\sigma - H_i P_\tau - M_i P_\sigma P_\tau)f(r, \mu_i)$$
$$+ t_0(1 + x_0 P^\sigma)\rho^{\alpha_0}(\mathbf{R})\delta(\mathbf{r})$$
$$+ t_3(1 + x_3 P^\sigma)\rho^{\alpha_3}(\mathbf{R})\delta(\mathbf{r}),\qquad(6)$$

where $\mathbf{r} = \mathbf{r}_1 - \mathbf{r}_2$ and $\mathbf{R} = (\mathbf{r}_1 + \mathbf{r}_2)/2$ are the relative and the center of mass coordinates. W_i, B_i, H_i, and M_i are the strengths of all the possible combinations of the spin (P^σ) and isospin exchange (P^τ) operators, respectively. μ_i are the ranges of the N form factor (Gaussian for Gogny, Yukawian for MDI or M3Y, and can be both for SEI) that describe the finite-range part of the force ($N = 1$ for MDI or SEI, $N = 2$ for Gogny, and $N = 3$ for M3Y). In Eq. (6) we have neglected the spin-orbit and tensor parts of the interaction owing to the fact that they do not contribute to the infinite nuclear matter.

In the case of warm symmetric nuclear matter described by a finite-range interaction given in Eq. (6), the single-particle energy is given by (see, for instance, Ref. [69])

$$\varepsilon(k) = \frac{\hbar^2 k^2}{2M} + \frac{3}{8}t_0\alpha_0 t_0\rho^{\alpha_0 - 1} + \frac{3}{8}\alpha_3 t_3\rho^{\alpha_3 - 1}$$
$$+ \sum_{i=1}^{N} g(0, \mu_i)\left[W_i + \frac{B_i}{2} - \frac{H_i}{2} - \frac{M_i}{4}\right]\rho$$

$$+ \sum_{i=1}^{N} \left[M_i + \frac{H_i}{2} - \frac{B_i}{2} - \frac{W_i}{4} \right]$$

$$\times \frac{\gamma}{(2\pi)^3} \int d\mathbf{k}' n(k') \tilde{g}(k, k', \mu_i), \qquad (7)$$

where $\tilde{g}(k, k', \mu_i)$ is the angular averaged Fourier transform of the finite-range form factor $f(\mathbf{r} - \mathbf{r}', \mu_i)$ [69] (see the Appendix for more details) and γ the degeneracy factor introduced before. The momentum distribution $n(k)$ in Eq. (7) is given by

$$n(k) = \frac{1}{e^{[\varepsilon(k) - \mu]/T} + 1}. \qquad (8)$$

At difference with the case of zero-range forces in which the integral of the momentum distribution $n(k)$ in Eq. (2) determines the effective chemical potential, in the case of finite-range forces one needs to solve the coupled system of Eqs. (7) and (8) with the constraint of Eq. (2), which for a given density allows to obtain the chemical potential μ. Once the Fermi-Dirac occupation number $n(k)$ is determined by this procedure, one can easily determine the energy density as

$$\mathcal{H} = \frac{\gamma}{(2\pi)^3} \int d\mathbf{k} \frac{\hbar^2 k^2}{2M} + \frac{3}{8} t_0 \rho^{\alpha_0} + \frac{3}{8} t_3 \rho^{\alpha_3}$$

$$+ \frac{1}{2} \sum_{i=1}^{N} g(0, \mu_i) \left[W_i + \frac{B_i}{2} - \frac{H_i}{2} - \frac{M_i}{4} \right] \rho^2$$

$$+ \sum_{i=1}^{N} \left[M_i + \frac{H_i}{2} - \frac{B_i}{2} - \frac{W_i}{4} \right]$$

$$\times \frac{\gamma^2}{2} \int \frac{d\mathbf{k}}{(2\pi)^3} n(k) \int \frac{d\mathbf{k}'}{(2\pi)^3} n(k') \tilde{g}(k, k', \mu_i), \quad (9)$$

and the entropy density as

$$\mathcal{S} = \gamma \int \frac{d\mathbf{k}}{(2\pi)^3} \{ n(k) \ln[n(k)] + [1 - n(k)] \ln[1 - n(k)] \}$$

$$= \frac{1}{T} \int \frac{d\mathbf{k}}{(2\pi)^3} n(k) \left[\varepsilon(k) + \frac{k}{3} \frac{d\varepsilon(k)}{dk} \right]. \qquad (10)$$

Finally, the pressure at a given temperature T is given by the standard thermodynamical relation

$$P_{\mathrm{FR}}(\rho, T) = \mu \rho - \mathcal{F} = \mu \rho - \mathcal{H} + \mathcal{S} T, \qquad (11)$$

where $\mathcal{F}$ is the free energy density.

It is important to mention here that in the case of SEI, the second density-dependent term in Eq. (9) is divided by a factor $(1 + b\rho)^{\alpha_3 - 2}$ and the contribution to the corresponding single-particle energy (7) is also modified accordingly. We label the SEI parametrizations used in this work by G or Y to indicate if the form factor is of the Gauss or Yukawa type and by the value of the corresponding incompressibility modulus. More details about these parametrizations can be found in Refs. [45,70].

III. ANALYSIS OF THE FINITE TEMPERATURE CALCULATIONS

Before discussing the results in detail, we make some general remarks about the nuclear matter properties of the models chosen for our study. The zero-range and finite-range mean-field models used in this study, in general, reproduce reasonably well binding energies and charge radii of finite nuclei and predict nuclear matter properties usually within the window of the empirical values, namely, energy per nucleon $e_0 = -15.8 \pm 0.5$ MeV, saturation density $\rho_0 = 0.16 \pm 0.01$ fm^{-3}, isoscalar effective mass ratio $m^* = M^*(\rho_0)/M = 0.6$–$1.0$, and incompressibility modulus $K_0 = 240 \pm 30$ MeV (see, for instance, Ref. [68]). We emphasize here the importance of the saturation density ρ_0, since it is directly related to the short-range nature of the nuclear force. Because of this feature, protons and neutrons only interact with their near surrounding nucleons and this mechanism leads to approximately constant value of ρ_0. Regarding the Gogny interactions considered in this work, we see that there are some parametrization with incompressibility modulus outside the window of the empirical values (see Table I). Among these the D1S interaction was fabricated to build up an accurate mass table [71]. The rest of the parametrizations with high K_0 values were built up in Ref. [72] in order to study the correlation between the incompressibility modulus in nuclear matter and the energy of the monopole vibrations. The isoscalar effective mass ratio m^* of the finite-range models considered in this work lie in the range of 0.6–0.7, which reproduce the excitation energy of the isoscalar giant quadrupole resonance [73]. This value of the isoscalar effective mass is in agreement with the value extracted from the optical model analysis of the nucleon-nucleus scattering [74]. Some of the Skyrme models which we have considered predict an effective mass close to the bare mass. Models with an effective mass ratio equal to or slightly larger than unity predict a single-particle level density close to the Fermi surface, which is in good agreement with the experiment without considering an additional particle-vibration coupling [75]. However, these models with effective mass close to the bare mass are prone to predict maximum masses of neutron stars below the lower limit of the observed value of $(2.01 \pm 0.04) M_\odot$ [68].

Since the pressure as a function of ρ and T of zero- and finite-range interactions is determined, as shown in Eqs. (5) and (11), it is now possible to analyze the critical parameters and the main features of the thermal symmetric nuclear matter for the different nonrelativistic models introduced in the previous section. Nevertheless, before that, a comment regarding the phase transition in nuclear systems is needed at this point. Conjectures concerning the existence of a liquid-gas phase transition in strongly interacting matter have been corroborated through indirect evidences, since the critical point itself cannot be directly observed in nuclear experiments. One of such evidences involves the distribution of the intermediate mass fragments produced, for instance, in the following reactions: ^{84}Kr + ^{197}Au [76], Au + C [77], Au + Al [77], Au + Cu [77], ^{197}Au + ^{197}Au [78], p + Xe [79], and p + Kr [79]. Another possible signature of the nuclear phase transition is identified from the analysis of the so-called caloric curve, or,

TABLE I. Critical parameters T_c (MeV), ρ_c (fm^{-3}), and P_c (MeV/fm^3), along with the quantities, namely, ρ_c/ρ_0, $Z_c = P_c/\rho_c T_c$, and the bulk parameters K_0 (MeV), $m^* = M^*(\rho_0)/M$, and ρ_0 (fm^{-3}) for different nonrelativistic parametrizations used in this work.

Model	T_c	ρ_c	P_c	$\frac{\rho_c}{\rho_0}$	Z_c	K_0	m^*	ρ_0
GSkI	15.09	0.052	0.223	0.328	0.284	230.21	0.776	0.159
GSkII	15.27	0.052	0.226	0.328	0.284	233.40	0.790	0.159
KDE0v1	14.86	0.054	0.225	0.330	0.279	227.54	0.744	0.165
LNS	14.93	0.057	0.235	0.328	0.275	210.78	0.826	0.175
MSL0	15.17	0.053	0.226	0.330	0.282	230.00	0.800	0.160
NRAPR	14.39	0.054	0.218	0.337	0.280	225.65	0.694	0.161
Ska25s20	16.27	0.053	0.239	0.329	0.278	220.75	0.980	0.161
Ska35s20	17.16	0.054	0.264	0.339	0.287	240.27	1.000	0.158
SKRA	14.36	0.052	0.208	0.329	0.276	216.98	0.748	0.159
SkT1	17.06	0.055	0.266	0.339	0.286	236.16	1.000	0.161
SkT2	17.04	0.055	0.265	0.339	0.286	235.73	1.000	0.161
SkT3	17.04	0.055	0.265	0.339	0.286	235.74	1.000	0.161
Skxs20	15.38	0.052	0.216	0.321	0.270	201.95	0.964	0.162
SQMC650	14.85	0.057	0.234	0.331	0.277	218.11	0.779	0.172
SQMC700	14.73	0.057	0.233	0.332	0.278	222.20	0.755	0.171
SV-sym32	16.03	0.053	0.242	0.332	0.285	233.81	0.900	0.159
Skχ414	18.33	0.059	0.311	0.349	0.286	243.18	1.075	0.170
Skχ450	17.08	0.053	0.261	0.341	0.287	239.54	1.006	0.156
Skχ500	18.20	0.059	0.305	0.349	0.285	238.16	1.087	0.168
SkΛ267	14.63	0.054	0.224	0.337	0.281	230.08	0.702	0.162
D1S	15.89	0.060	0.281	0.368	0.295	202.88	0.697	0.163
D1M	15.95	0.058	0.272	0.352	0.294	224.98	0.746	0.165
D1N	15.76	0.056	0.261	0.348	0.296	225.65	0.747	0.161
D250	17.16	0.061	0.332	0.386	0.318	249.54	0.702	0.158
D260	15.48	0.059	0.273	0.369	0.299	259.49	0.615	0.160
D280	15.21	0.058	0.263	0.379	0.298	285.19	0.575	0.153
D300	16.80	0.058	0.310	0.372	0.318	299.14	0.681	0.156
MDI	15.62	0.058	0.268	0.363	0.296	210.98	0.673	0.160
M3Y-P1	15.78	0.062	0.294	0.367	0.301	225.70	0.641	0.169
M3Y-P2	15.66	0.059	0.277	0.363	0.300	220.40	0.652	0.163
M3Y-P3	16.12	0.060	0.290	0.369	0.300	245.80	0.658	0.163
M3Y-P4	16.08	0.060	0.294	0.369	0.304	235.30	0.665	0.163
M3Y-P5	15.78	0.060	0.289	0.369	0.305	235.60	0.629	0.163
M3Y-P4$'$	15.91	0.060	0.290	0.369	0.304	230.40	0.653	0.163
M3Y-P5$'$	15.88	0.060	0.291	0.369	0.306	239.10	0.637	0.163
M3Y-P6	15.97	0.061	0.306	0.375	0.314	239.70	0.596	0.163
M3Y-P7	16.33	0.062	0.326	0.381	0.322	254.70	0.589	0.163
SEIG263	16.30	0.056	0.278	0.361	0.305	262.52	0.712	0.155
SEIG245	15.79	0.055	0.260	0.350	0.300	245.62	0.711	0.157
SEIG227	15.23	0.055	0.242	0.344	0.289	227.64	0.710	0.160
SEIG207	14.55	0.054	0.221	0.333	0.281	207.69	0.709	0.162
SEIY282	17.35	0.061	0.340	0.379	0.321	282.30	0.686	0.161
SEIY254	16.43	0.058	0.298	0.360	0.313	253.68	0.686	0.161
SEIY238	15.88	0.058	0.275	0.360	0.298	237.52	0.686	0.161
SEIY220	15.26	0.055	0.250	0.342	0.298	219.87	0.686	0.161

in other words, the dependence of temperature on the excitation energy per particle in finite nuclei. It was first predicted theoretically in Ref. [80] and later discovered by the ALADIN Collaboration [81], from a fragment distributions study produced in Au + Au collisions at incident energy of 600 MeV per nucleon. The plateau exhibited by this curve is characteristic of systems presenting phase transitions, thus supporting the existence of such thermodynamical phenomenology in nuclear systems [82].

We start by showing in Table I the critical parameters P_c, ρ_c, and T_c along with ρ_c/ρ_0, the compressibility factor $Z_c = P_c/\rho_c T_c$, and some bulk parameters, namely, incompressibility K_0, isoscalar effective mass ratio m^* (at $\rho = \rho_0$), and the saturation density itself (ρ_0). Concerning the ratio Z_c, one can verify that all parametrizations present Z_c smaller than the respective value related to the van der Waals model, namely, 0.375. This is a feature also observed for relativistic models, as pointed out, for instance, in Refs. [10,83]. Notice that
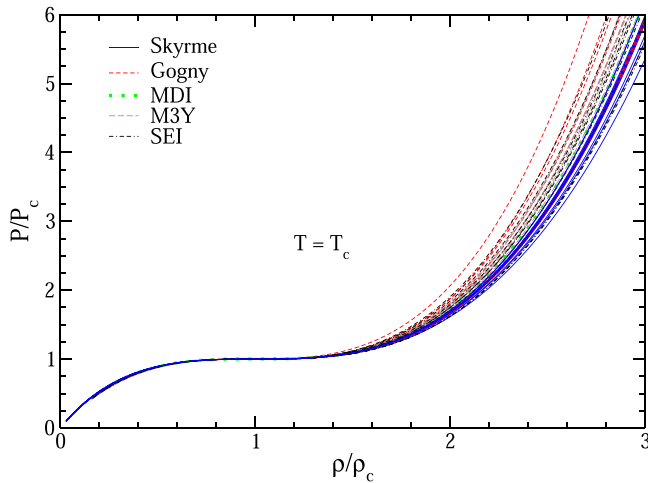
FIG. 1. P/P_c as a function of ρ/ρ_c for the nonrelativistic parametrizations. All isotherms are calculated at $T = T_c$.

FIG. 2. Values of (a) P_c and (b) ρ_c for the parametrizations of the Skyrme, Gogny, MDI, M3Y, and SEI models in comparison with the corresponding experimental values extracted from Ref. [84] (ranges limited by the horizontal dashed lines).

Table I enlists, for the first time, to the best of our knowledge, the critical parameters T_c, P_c, and ρ_c for almost all the nonrelativistic finite-range effective nucleon-nucleon interactions available in the literature.

In Fig. 1 we present the critical isotherms, i.e., pressure as a function of density scaled by their critical values at $T = T_c$ for different types of parametrizations considered in this work. It is clear that such scaled curves are indistinguishable in the gaseous phase ($\rho < \rho_c$), and model dependent for the liquid phase ($\rho > \rho_c$), where the interactions become more important due to the closer proximity between the nucleons. Previously, this finding was observed only for those parametrizations of the relativistic mean-field models which contain self-interactions in the scalar field σ (Boguta-Bodmer model) [83]. Later on, in Ref. [10], it was investigated in a more sophisticated version of the RMF model including quartic self-interaction in the vector field ω_μ, interactions between scalar and vector fields (σ and ω_μ), and interactions between scalar and isovector fields (σ and $\vec{\rho}_\mu$). The same pattern was observed also for those parametrizations. Here we observe similar findings once again for the nonrelativistic models. This strongly suggests towards a universality in the isotherms of symmetric nuclear matter for hadronic models, i.e., model independence in the gaseous region and distinguishability among the different interactions in the liquid phase.

Concerning the critical parameters calculated for the different nonrelativistic parametrizations explored here, we compare our results with experimental and theoretical predictions available in the literature. An experimental study given in Ref. [84] provides values for all three quantities, namely, $T_c = 17.9 \pm 0.4$ MeV, $P_c = 0.31 \pm 0.07$ MeV/fm^3, and $\rho_c = 0.06 \pm 0.01$ fm^{-3}. For this purpose, the authors analyzed data from compound-nucleus and nuclear multifragmentation [85,86]. In Fig. 2 we display the outcomes related to P_c and ρ_c obtained for all nonrelativistic parametrizations used in this work. As one can see, all the finite-range parametrizations of the Gogny, MDI, M3Y, and SEI types are in full agreement with the experimental ranges of Ref. [84] for P_c and ρ_c. However, the Skyrme parametrizations are also inside
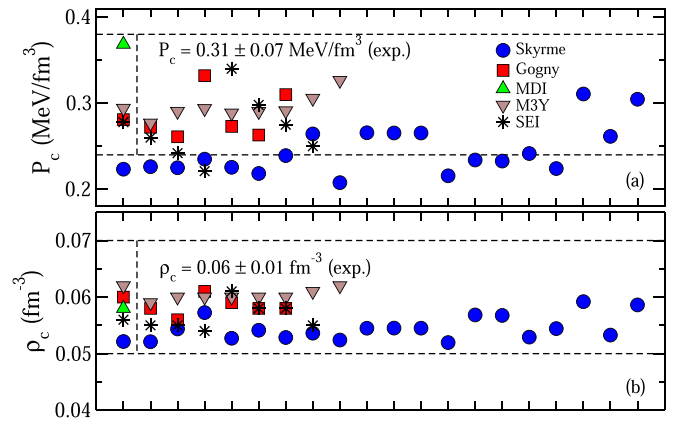
the range of ρ_c but not all of them are compatible with the P_c values. Ten out of 20, namely, GSkI, GSkII, KDE0v1, MSL0, NRAPR, SKRA, Skxs20, SQMC650, SQMC700, and SkΛ267, lie below the lower experimental limit for this quantity. It is important to mention that the effective mass seems to play an important role in this case. Notice that with the exception of Skxs20, all the remaining parametrizations mentioned just above present $m^* \leqslant 0.80$.

In Fig. 3 we display the values of T_c calculated from the models analyzed in this work along with their different experimental values for comparison. As one can see from this figure, the nonrelativistic parametrizations predict T_c compatible with experimental values of Refs. [4,84,87–91]. Furthermore, we also observe agreement between the results obtained with different nonrelativistic parametrizations and the ones obtained with different theoretical models in Refs. [10,92]. Actually,
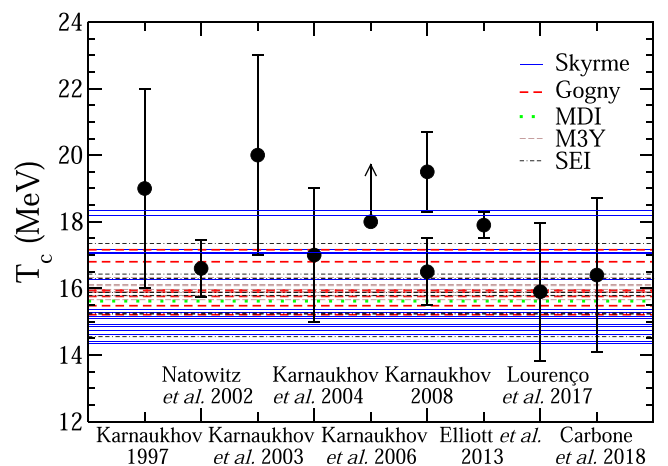
FIG. 3. Values of T_c for the nonrelativistic parametrizations compared with experimental and theoretical data (circles) collected from Karnaukhov, 1997 [87]; Natowitz *et al.*, 2002 [4]; Karnaukhov *et al.*, 2003 [88]; Karnaukhov *et al.*, 2004 [89]; Karnaukhov *et al.*, 2006 [90]. Karnaukhov, 2008 [91]. Elliott *et al.* 2013, [84]. Lourenço *et al.*, 2017 [10]. and Carbone *et al.*, 2018 [92].
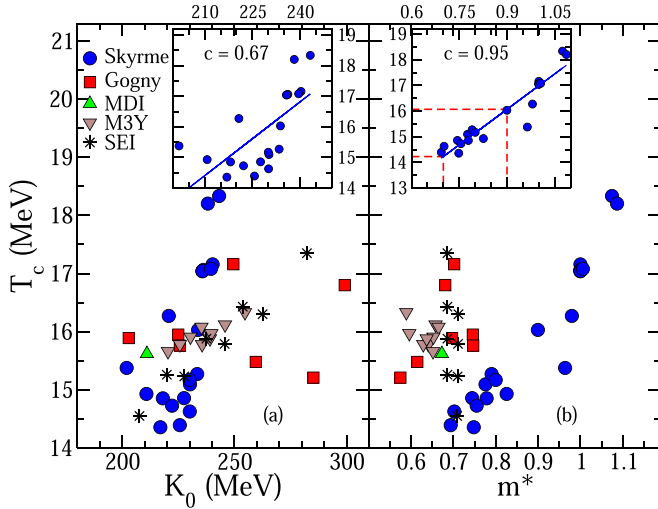
FIG. 4. T_c as a function of (a) K_0 and (b) m^* for the nonrelativistic models used in this work. Solid lines in the insets: fitting curves related to the Skyrme parametrizations, with correlation coefficients given by (a) $c = 0.67$ and (b) $c = 0.95$ (see text for more details).

TABLE II. Correlation coefficients (c) among different pairs of critical parameters and nuclear matter properties are listed for four families of nonrelativistic interactions considered in this work along with combining them together in "All."

c	Skyrme	Gogny	M3Y	SEI	All
$T_c \times K_0$	0.67	0.13	0.89	0.98	0.44
$T_c \times m^*$	0.95	0.45	−0.37	−0.43	0.51
$P_c \times K_0$	0.68	0.26	0.78	0.93	0.58
$P_c \times m^*$	0.83	0.16	−0.81	−0.56	−0.20
$\rho_c \times K_0$	0.17	−0.11	0.42	0.80	0.33
$\rho_c \times m^*$	0.26	−0.16	−0.64	−0.67	0.49
$T_c \times P_c$	0.95	0.94	0.79	0.98	0.72

the critical temperatures provided by the nonrelativistic interactions analyzed in this work agree better with experimental values than in those of some RMF models (see Fig. 2 of Ref. [10]). In Ref. [10], the authors calculated T_c for a class of RMF models [93] containing nonlinear σ and ω_μ terms and crossing terms involving these fields (30 parametrizations), and for RMF models in which couplings are density dependent (4 parametrizations); all of them are consistent with nuclear matter constraints. In Ref. [92], calculations were performed by using two- and three-body nuclear interactions consistently derived through chiral effective field theory. A van der Waals pattern was also observed in such models [92].

Another interesting investigation on the warm nuclear matter is the search for possible correlations between bulk parameters of symmetric nuclear matter (SNM), evaluated at $\rho = \rho_0$, and the critical parameters. This feature can be useful in order to consolidate the constraints on T_c, P_c, and ρ_c. In Ref. [10], for instance, it was shown that the consistent RMF models exhibit a general trend of correlation between the critical parameters and the incompressibility coefficient K_0. For the nonrelativistic parametrizations used here, we present T_c as a function of K_0 and m^* in Fig. 4. One can notice an increasing trend of T_c as a function of both K_0 and m^* for the Skyrme parametrizations. The correlation coefficients are 0.67 and 0.95 for K_0 and m^*, respectively. The results observed for the Skyrme models are in line with other studies performed with different hadronic models. For instance, in Ref. [94] the same correlation of Fig. 4(a) is found for a class of real gas models used to describe symmetric nuclear matter at finite temperature, after a suitable conversion of these classical models into quantum ones through the incorporation of the Fermi-Dirac distribution function in the momentum integrals. Furthermore, we also observe qualitative agreement with other theoretical calculations that provide analytical expressions of T_c as a function of K_0, as in Refs. [4,95–97]. With regard to the T_c as a function of m^*, we remark that a

systematic study was performed with parametrizations of the RMF model with third- and fourth-order self-interactions in the scalar field σ [98]. For these models, we remind the reader that m^* is the Dirac effective mass, which is slightly different from the quantity defined in the nonrelativistic approach used in the present paper. In Ref. [98], in which it was also observed that T_c depends on K_0, the authors verified a clear relationship between T_c and m^*. However, in these models only the variation of m^* was taken into account; i.e., saturation density, binding energy, and incompressibility were kept fixed. Regarding the finite-range models, we can see that the SEI family of parametrizations, which have very similar nuclear matter properties except incompressibility, show a very clear correlation between T_c and K_0 with a correlation coefficient of 0.98 (see Table II). This correlation is also observed in the M3Y parametrizations where a correlation coefficient of 0.89 was found. Concerning the relation between the T_c and m^*, the predictions of the finite-range interactions, in particular SEI and M3Y, and the ones of the Skyrme forces are clearly different. The SEI interactions, and to some extent the M3Y ones, have almost the same effective mass and there is no correlation between T_c and m^*. This situation is different from the one found with the Skyrme forces, where a clear linear correlation is observed [see the inset of Fig. 4(b)]. However, Gogny forces, which have properties in symmetric nuclear matter quite different among them, do not show any clear correlation between T_c and K_0 or m^* (see also Ref. [97] in this respect).

One needs to be careful in a correlation study like the present one. Some of the finite-range interactions used in the present work were obtained in a systematic way to satisfy certain constraints. Their merits should not be tested only with a correlation study. However, most of the Skyrme parametrizations used in the present work satisfy several independent constraints imposed by experiments and astronomical observations (see Ref. [49]). An independent correlation study is quite justified using only these Skyrme interactions. In the inset of Fig. 4(b) one can see a positive linear correlation between T_c and m^*. If we take a conservative estimate of m^* of 0.7–0.9, it translates into a variation of T_c from 14.225 to 16.066 MeV, as T_c and m^* show a high positive correlation between them. These are indicated by the red parallel lines to the axes in the inset of Fig. 4(b).
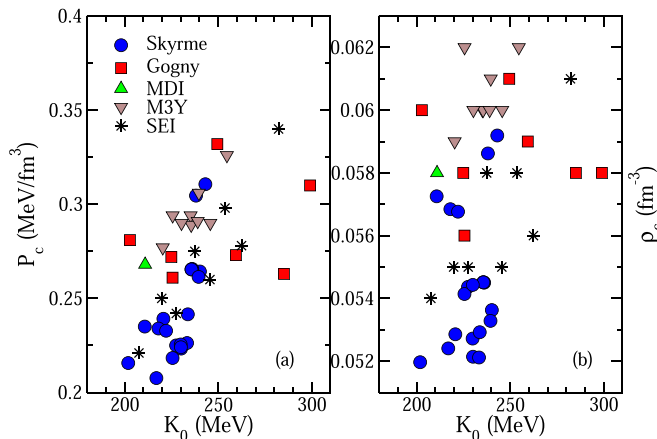
FIG. 5. Critical (a) pressure and (b) density as a function of K_0 for the different Skyrme, Gogny, MDI, M3Y, and SEI parametrizations considered in this work (see text for details).

The influence of K_0 on P_c and ρ_c is analyzed in Fig. 5. The behavior of P_c and ρ_c as increasing functions of K_0 was also observed for the RMF models investigated in Refs. [10,98]. From Fig. 5 we can still appreciate the correlations between P_c and K_0, in particular for the SEI and M3Y forces and less clearly for the Skyrme interactions. This is confirmed by the correlation coefficients reported in Table II. From Fig. 5(a) and Table II it is again clear that Gogny forces do not show P_c-K_0 correlation. The results reported in Table II also show that there is no correlation between K_0 or m^* and ρ_c.

Finally, we display in Fig. 6 the relationship between T_c and P_c. For the classical van der Waals model, one has $T_c = 8bP_c$ with b being the excluded volume parameter (strength of the repulsive interaction), indicating a clear linear relation. For the nonrelativistic models studied here, an increment of T_c as a function of P_c is observed with some deviation from the exact linear pattern. A much more clear linear behavior was observed, for instance, with the RMF parametrizations
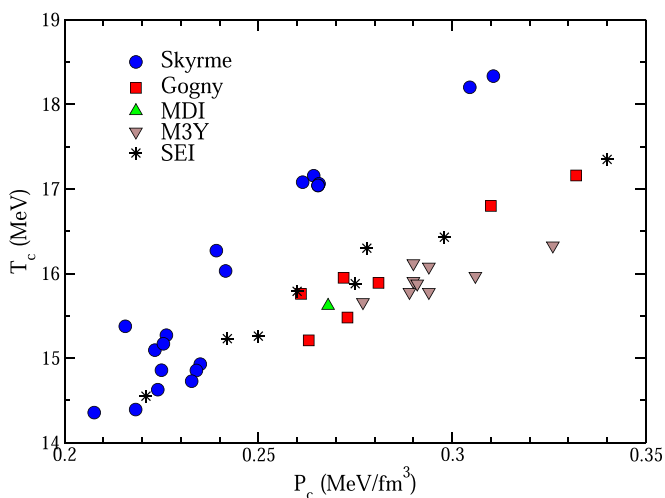
FIG. 6. T_c as a function of P_c for the different Skyrme, Gogny, MDI, M3Y, and SEI parametrizations considered in this work (see text for more details).

and density-dependent RMF Hartree-Fock models used in Ref. [99]. All the finite-range models follow the T_c-P_c correlation quite precisely as it can be seen from Fig. 6 and from the correlation coefficients given in Table II. Regarding the Skyrme results, we see that the models which predict a critical pressure below 0.24 MeV fm^{-3} and at the same time have a small effective mass m^* below 0.8 are well aligned with the finite-range ones. We also see that the remaining Skyrme parametrizations, which have an effective mass close to the bare mass, lie on top with another parallel line shifted to higher critical temperature. As a consequence, our study predicts that the T_c-P_c correlation is reinforced for models with similar effective mass. One can notice that the Skyrme models just mentioned above with m^* greater than 0.8 reproduce better the experimental constraint on the critical pressure P_c (see Fig. 2 and corresponding discussion). However, they follow a different T_c-P_c correlation line compared to the rest of models considered in this work, including the ones of the Skyrme family (see Fig. 6).

IV. SUMMARY AND CONCLUSIONS

In this work we have analyzed symmetric nuclear matter at finite temperature for a set of parametrizations of the Skyrme, Gogny, MDI, M3Y, and SEI nonrelativistic models. For the first one, we have chosen the so-called consistent Skyrme parametrizations (CSkPs), namely, GSkI, GSkII, KDE0v1, LNS, MSL0, NRAPR, Ska25s20, Ska35s20, SKRA, Skxs20, SQMC650, SQMC700, SkT1, SkT2, SkT3, and SV-sym32. They satisfy a set of constraints related to the nuclear matter and pure neutron matter [49]. Furthermore, they are also consistent with the boundaries of the tidal deformabilities determined by the LIGO and Virgo Collaboration studies, all of them related to the detection of gravitational waves coming from the neutron star merger event GW170817 [63]. For the finite-range models, we have chosen some representative parametrizations. We also furnished the expressions for the pressure as a function of temperature and density for the considered models [see Eqs. (5) and (11)]. Once this thermodynamic quantity was determined, it was possible to find the critical parameters (CPs) of the models, namely, T_c, P_c, and ρ_c, by imposing the conditions given in Eq. (4). The respective values of these quantities are listed in Table I. To the best of our knowledge, assemblies of critical properties of nuclear matter at finite temperature of this sort are quite scarce in the literature for finite-range interactions.

One of the results found in our investigation is the pattern exhibited in Fig. 1, namely, all isotherms collapse in the low-density region (gaseous phase), and nuclear interactions become important for densities greater than ρ_c (liquid phase). Such a feature was also observed in Ref. [83] in which the calculations were restricted to the relativistic mean-field (RMF) model presenting third- and fourth-order self-interactions in the scalar field. In Ref. [10], the same phenomenology was observed for more sophisticated versions of the RMF models including quartic self-interaction in the vector field and other mesonic interactions. Our finding strongly suggests a kind of universality for the isotherms of the hadronic models (relativistic and nonrelativistic) for symmetric nuclear matter.

With regard to the values of the CPs of the studied nonrelativistic parametrizations, we found very good agreement of all the models with the experimental value of $\rho_c = 0.06 \pm 0.01$ fm^{-3} [84]. All the finite-range models considered here, as well as 10 out of 20 Skyrme parametrizations analyzed, lie within the experimental limit of $P_c = 0.31 \pm 0.07$ MeV/fm^3 [84]. Finally, concerning T_c, we have compared our results with both theoretical and experimental data collected from the literature. Figure 3 shows that all the models analyzed here are compatible with the experimental values. We have also verified that the critical parameters obtained here are also compatible with previous theoretical results reported in Refs. [10,92], in which the authors have used a class of RMF models [10], and with the nuclear models derived from chiral effective field theory [92].

Another investigation performed in this work was the search for possible correlations between bulk parameters, evaluated at the saturation density, and the CPs. In Table II we have shown the correlation coefficients obtained for some possible relationships. The general trend of T_c as an increasing function of K_0 was found for all families of models individually with the exception of the Gogny parametrizations. This finding is compatible with studies using other hadronic models [4,94–98]. In Fig. 5(a) and in Table II, where the correlation coefficient for the $P_c \times K_0$ relationship was presented, we observed the same pattern, namely, P_c and K_0 are correlated to each other for all models except for the Gogny ones. This particular correlation was also exhibited for relativistic parametrizations explored in Refs. [10,98]. With regard to ρ_c as a function of K_0, we find a good correlation coefficient only for the parametrizations of the SEI model, namely, $c = 0.80$. Concerning the critical parameters as a function of m^*, we found hints of correlation for Skyrme (T_c and P_c), M3Y (P_c and ρ_c), and SEI (ρ_c) models. Finally, in Fig. 6 we verified correlation between T_c and P_c in agreement with other findings [99]. Also our results seem to point out that this specific correlation is better fulfilled for models with similar effective mass independently of the type of interaction considered.

APPENDIX

In momentum space, the finite-range interaction is given by the Fourier transform of the form factor in coordinate space, $f(s, \mu)$, where $s = |\mathbf{r} - \mathbf{r}'|$ and μ is the range of the force, and, therefore,

$$g(|\mathbf{k} - \mathbf{k}'|, \mu) = \int d\mathbf{s} e^{i(\mathbf{k}-\mathbf{k}')\mathbf{s}} f(s, \mu). \quad (A1)$$

The interaction in momentum space depends on the modulus of the relative momentum and therefore on the angle between $\mathbf{k}$ and $\mathbf{k}'$. We can finally write the interaction with spherical symmetry in momentum space by performing the angular average:

$$\tilde{g}(k, k', \mu) = \frac{1}{4\pi} \int d\Omega g(\sqrt{k^2 + k'^2 - 2kk'\cos\theta}). \quad (A2)$$

In this work we use Gaussian $f_G(s) = e^{-s^2/\mu^2}$ and Yukawian $f_Y(s) = e^{-\mu s}/\mu s$ form factors. The corresponding Fourier transforms are

$$g_G(|\mathbf{k} - \mathbf{k}'|, \mu) = (\sqrt{\pi}\mu)^3 e^{-\frac{\mu^2(\mathbf{k}-\mathbf{k}')^2}{4}} \quad (A3)$$

and

$$g_Y(|\mathbf{k} - \mathbf{k}'|, \mu) = \frac{4\pi}{\mu} \frac{1}{\mu^2 + (\mathbf{k} - \mathbf{k}')^2}. \quad (A4)$$

After the angular average they become

$$\tilde{g}_G(k, k', \mu) = \frac{2\pi^{3/2}\mu}{kk'} e^{-\frac{\mu^2(k^2+k'^2)}{4}} \sinh\frac{\mu kk'}{2} \quad (A5)$$

and

$$\tilde{g}_Y(k, k', \mu) = \frac{\pi}{\mu kk'} \ln\frac{\mu^2 + (k + k')^2}{\mu^2 + (k - k')^2}, \quad (A6)$$

which enter in Eqs. (7) and (9).

[1] P. Chomaz, M. Colonna, and J. Randrup, Phys. Rep. **389**, 263 (2004).

[2] C. Das, S. D. Gupta, W. Lynch, A. Mekjian, and M. Tsang, Phys. Rep. **406**, 1 (2005).

[3] B. Borderie and J. D. Frankland, Prog. Part. Nucl. Phys. **105**, 82 (2019).

[4] J. B. Natowitz, K. Hagel, Y. Ma, M. Murray, L. Qin, R. Wada, and J. Wang, Phys. Rev. Lett. **89**, 212701 (2002).

[5] C. Sfienti, P. Adrich, T. Aumann, C. O. Bacri, T. Barczyk, R. Bassini, S. Bianchin, C. Boiano, A. S. Botvina, A. Boudard *et al.* (ALADIN2000 Collaboration), Phys. Rev. Lett. **102**, 152701 (2009).

[6] A. F. Fantina, S. De Ridder, N. Chamel, and F. Gulminelli, Astron. Astrophys. **633**, A149 (2020).

[7] T. Carreau, F. Gulminelli, N. Chamel, A. F. Fantina, and J. M. Pearson, Astron. Astrophys. **635**, A84 (2020).

[8] J. M. Lattimer and M. Prakash, Phys. Rep. **621**, 127 (2016).

[9] A. S. Schneider, L. F. Roberts, and C. D. Ott, Phys. Rev. C **96**, 065802 (2017).

[10] O. Lourenço, M. Dutra, and D. P. Menezes, Phys. Rev. C **95**, 065212 (2017).

[11] C. F. von Weizsäcker, Z. Phys. **96**, 431 (1935).

[12] D. Benzaid, S. Bentridi, A. Kerraci, and N. Amrani, Nucl. Sci. Tech. **31**, 9 (2020).

[13] R. Machleidt and D. R. Entem, Phys. Rep. **503**, 1 (2011).

[14] R. Machleidt and F. Sammarruca, Phys. Scr. **91**, 083007 (2016).

[15] T. R. Whitehead, Y. Lim, and J. W. Holt, Phys. Rev. C **101**, 064613 (2020).

[16] P.-G. Reinhard, Rep. Prog. Phys. **52**, 439 (1989).

[17] D. Vretenar, A. V. Afanasjev, G. A. Lalazissis, and P. Ring, Phys. Rep. **409**, 101 (2005).

[18] B.-A. Li, L.-W. Chen, and C. Ming Ko, Phys. Rep. **464**, 113 (2008).

[19] D. Vretenar, T. Niksic, and P. Ring, Phys. Rev. C **68**, 024310 (2003).

[20] T. H. R. Skyrme, Philos. Mag. **1**, 1043 (1956).

[21] T. H. R. Skyrme, Nucl. Phys. **9**, 615 (1959).

[22] J. S. Bell and T. H. R. Skyrme, Philos. Mag. **1**, 1055 (1956).

[23] T. H. R. Skyrme, in *Proceedings of the Rehovoth Conference on Nuclear Structure* (North-Holland, Amsterdam, 1958), p. 20.

[24] J. R. Stone and P.-G. Reinhard, Prog. Part. Nucl. Phys. **58**, 587 (2007).

[25] G. Sauer, H. Chandra, and U. Mosel, Nucl. Phys. A **264**, 221 (1976).

[26] L. Guo-Quiang, J. Phys. G **17**, 1 (1991).

[27] J. Dechargé and D. Gogny, Phys. Rev. C **21**, 1568 (1980).

[28] J.-F. Berger, M. Girod, and D. Gogny, Comput. Phys. Commun. **63**, 365 (1991).

[29] F. Chappert, M. Girod, and S. Hilaire, Phys. Lett. B **668**, 420 (2008).

[30] S. Goriely, S. Hilaire, M. Girod, and S. Péru, Phys. Rev. Lett. **102**, 242501 (2009).

[31] R. Sellahewa and A. Rios, Phys. Rev. C **90**, 054327 (2014).

[32] C. Gonzalez-Boquera, M. Centelles, X. Viñas, and A. Rios, Phys. Rev. C **96**, 065806 (2017).

[33] C. Gonzalez-Boquera, M. Centelles, X. Viñas, and L. M. Robledo, Phys. Lett. B **779**, 195 (2018).

[34] C. Mondal, X. Viñas, M. Centelles, and J. N. De, Phys. Rev. C **102**, 015802 (2020).

[35] C. Gale, G. Bertsch and S. Das Gupta, Phys. Rev. C **35**, 1666 (1987).

[36] C. B. Das, S. Das Gupta, C. Gale and B.-A. Li, Phys. Rev. C **67**, 034611 (2003).

[37] J. Xu, L. W. Chen, B. A. Li, and H.-R. Ma, Astrophys. J. **697**, 1549 (2009).

[38] G. Bertsch, J. Borysowicz, H. MacManus, and W. G. Love, Nucl. Phys. A **284**, 399 (1977).

[39] H. Nakada, Phys. Rev. C **68**, 014316 (2003).

[40] H. Nakada, Phys. Rev. C **78**, 054301 (2008).

[41] H. Nakada, Phys. Rev. C **81**, 027301 (2010).

[42] H. Nakada, Phys. Rev. C **87**, 014336 (2013).

[43] D. T. Khoa, W. von Oertzen, and A. A. Ogloblin, Nucl. Phys. A **602**, 98 (1996); D. T. Khoa, G. R. Satchler, and W. von Oertzen, Phys. Rev. C **56**, 954 (1997).

[44] B. Behera, T. R. Routray, and R. K. Satpathy, J. Phys. G **24**, 2073 (1998).

[45] B. Behera, X. Viñas, T. R. Routry, and M. Centelles, J. Phys. G **42**, 045103 (2015).

[46] B. Behera, X. Viñas, M. Bhuyan, T. R. Routry, B. K. Sharma, and S. K. Patra, J. Phys. G **40**, 095105 (2013).

[47] B. Behera, X. Viñas, T. R. Routry, L. M. Robledo, M. Centelles, and S. P. Pattnaik, J. Phys. G **43**, 045115 (2016).

[48] J. M. Lattimer and D. G. Ravenhall, Astrophys. J. **223**, 314 (1978).

[49] M. Dutra, O. Lourenço, J. S. Sá Martins, A. Delfino, J. R. Stone, and P. D. Stevenson, Phys. Rev. C **85**, 035201 (2012).

[50] S. J. Lee and A. Z. Mekjian, Phys. Rev. C **63**, 044605 (2001).

[51] R. K. Su, S. D. Yang, and T. T. S. Kuo, Phys. Rev. C **35**, 1539 (1987).

[52] B. K. Agrawal, S. K. Dhiman, and R. Kumar, Phys. Rev. C **73**, 034319 (2006).

[53] B. K. Agrawal, S. Shlomo, and V. K. Au, Phys. Rev. C **72**, 014310 (2005).

[54] L. G. Cao, U. Lombardo, C. W. Shen, and N. V. Giai, Phys. Rev. C **73**, 014313 (2006).

[55] L. W. Chen, C. M. Ko, B.-A. Li, and J. Xu, Phys. Rev. C **82**, 024321 (2010).

[56] A. W. Steiner, M. Prakash, J. M. Lattimer, and P. J. Ellis, Phys. Rep. **411**, 325 (2005).

[57] B. A. Brown (private communication).

[58] M. Rashdan, Mod. Phys. Lett. A **15**, 1287 (2000).

[59] B. A. Brown, G. Shen, G. C. Hillhouse, J. Meng, and A. Trzcińska, Phys. Rev. C **76**, 034305 (2007).

[60] P. A. M. Guichon, H. H. Matevosyan, N. Sandulescu, and A. W. Thomas, Nucl. Phys. A **772**, 1 (2006).

[61] F. Tondeur, M. Brack, M. Farine, and J. M. Pearson, Nucl. Phys. A **420**, 297 (1984).

[62] P. Klüpfel, P.-G. Reinhard, T. J. Bürvenich, and J. A. Maruhn, Phys. Rev. C **79**, 034310 (2009).

[63] O. Lourenço, M. Dutra, C. H. Lenzi, S. K. Biswal, M. Bhuyan, and D. P. Menezes, Eur. Phys. J. A **56**, 32 (2020).

[64] B. P. Abbott *et al.* (LIGO Scientific Collaboration and Virgo Collaboration), Phys. Rev. Lett. **119**, 161101 (2017).

[65] B. P. Abbott *et al.* (LIGO Scientific Collaboration and Virgo Collaboration), Phys. Rev. Lett. **121**, 161101 (2018).

[66] B. P. Abbott *et al.* (LIGO Scientific Collaboration and Virgo Collaboration), Phys. Rev. X **9**, 011001 (2019).

[67] Y. Lim and J. W. Holt, Phys. Rev. C **95**, 065805 (2017).

[68] T. Malik, B. K. Agrawal, J. N. De, S. K. Samaddar, C. Providência, C. Mondal, and T. K. Jha, Phys. Rev. C **99**, 052801(R) (2019).

[69] H. Kucharek, P. Ring, and P. Schuck, Z. Phys. A **334**, 119 (1989).

[70] T. R. Routray, X. Viñas, D. N. Basu, S. P. Pattnaik, M. Centelles, L. M. Robledo, and B. Behera, J. Phys. G **43**, 105101 (2016).

[71] AMEDEE database, doi: 10.1051/ndata:07709.

[72] J. P. Blaizot, J. F. Berger, J. Dechargé, and M. Girod, Nucl. Phys. A **591**, 435 (1995).

[73] O. Bohigas, A. Lane, and J. Martorell, Phys. Rep. **51**, 267 (1979).

[74] X.-H. Li, W.-J. Guo, B.-A. Li, L.-W. Chen, F. J. Fattoyev, and W. G. Newton, Phys. Lett. B **743**, 408 (2015).

[75] A. K. Dutta, J.-P. Arcoragi, J. M. Pearson, R. Behnnan, and F. Tondeur, Nucl. Phys. A **458**, 77 (1986).

[76] G. F. Peaslee, M. B. Tsang, C. Schwarz, M. J. Huang, W. S. Huang, W. C. Hsi, C. Williams, W. Bauer, D. R. Bowman, M. Chartier *et al.*, Phys. Rev. C **49**, R2271(R) (1994).

[77] C. A. Ogilvie, J. C. Adloff, M. Begemann-Blaich, P. Bouissou, J. Hubele, G. Imme, I. Iori, P. Kreutz, G. J. Kunde, S. Leray *et al.*, Phys. Rev. Lett. **67**, 1214 (1991).

[78] M. B. Tsang, W. C. Hsi, W. G. Lynch, D. R. Bowman, C. K. Gelbke, M. A. Lisa, G. F. Peaslee, G. J. Kunde, M. L. Begemann-Blaich, T. Hofmann *et al.*, Phys. Rev. Lett. **71**, 1502 (1993).

[79] J. E. Finn, S. Agarwal, A. Bujak, J. Chuang, L. J. Gutay, A. S. Hirsch, R. W. Minich, N. T. Porile, R. P. Scharenberg, B. C. Stringfellow, and F. Turkot, Phys. Rev. Lett. **49**, 1321 (1982).

[80] J. Bondorf, R. Donangelo, I. N. Mishustin, and H. Schulz, Nucl. Phys. A **444**, 460 (1985).

[81] J. Pochodzalla, T. Mohlenkamp, T. Rubehn, A. Schuttauf, A. Worner, E. Zude, M. Begemann-Blaich, Th. Blaich, H. Emling, A. Ferrero *et al.*, Phys. Rev. Lett. **75**, 1040 (1995).

[82] J. B. Natowitz, R. Wada, K. Hagel, T. Keutgen, M. Murray, A. Makeev, L. Qin, P. Smith, and C. Hamilton, Phys. Rev. C **65**, 034618 (2002).

[83] J. B. Silva, O. Lourenço, A. Delfino, J. S. Sá Martins, and M. Dutra, Phys. Lett. B **664**, 246 (2008).

[84] J. B. Elliott, P. T. Lake, L. G. Moretto, and L. Phair, Phys. Rev. C **87**, 054622 (2013).

[85] T. S. Fan *et al.*, Nucl. Phys. A **679**, 121 (2000).

[86] V. E. Viola, K. Kwiatkowski, L. Beaulieu, D. S. Bracken, H. Breuer, J. Brzychczyk, R. T. de Souza, D. S. Ginger, W-C. Hsi, R. G. Korteling *et al.*, Phys. Rep. **434**, 1 (2006); K. Kwiatkowski, D. S. Bracken, K. B. Morley, J. Brzychczyk, E. Renshaw Foxford, K. Komisarcik, V. E. Viola, N. R. Yoder, J. Dorsett, J. Poehlman, N. Madden, and J. Ottarson, Nucl. Instrum. Methods Phys. Res. Sect. A **360**, 571 (1995); T. Lefort, K. Kwiatkowski, W.-c. Hsi, L. Pienkowski, L. Beaulieu, B. Back, H. Breuer, S. Gushue, R. G. Korteling, R. Laforest *et al.*, Phys. Rev. Lett. **83**, 4033 (1999); L. Beaulieu, T. Lefort, K. Kwiatkowski, R. T. de Souza, W.-c. Hsi, L. Pienkowski, B. Back, D. S. Bracken, H. Breuer, E. Cornell *et al.*, *ibid.* **84**, 5971 (2000); L. Beaulieu, T. Lefort, K. Kwiatkowski, W.-c. Hsi, L. Pienkowski, R. G. Korteling, R. Laforest, E. Martin, E. Ramakrishnan, D. Rowland *et al.*, Phys. Rev. C **63**, 031302(R) (2001).

[87] V. A. Karnaukhov, Phys. At. Nucl. **60**, 1625 (1997).

[88] V. A. Karnaukhov *et al.*, Phys. Rev. C **67**, 011601(R) (2003).

[89] V. A. Karnaukhov *et al.*, Nucl. Phys. A **734**, 520 (2004).

[90] V. A. Karnaukhov *et al.*, Nucl. Phys. A **780**, 91 (2006).

[91] V. A. Karnaukhov, Phys. At. Nucl. **71**, 2067 (2008).

[92] A. Carbone, A. Polls, and A. Rios, Phys. Rev. C **98**, 025804 (2018).

[93] O. Lourenço, M. Dutra, C. H. Lenzi, C. V. Flores, and D. P. Menezes, Phys. Rev. C **99**, 045202 (2019).

[94] V. Vovchenko, Phys. Rev. C **96**, 015206 (2017).

[95] J. Kapusta, Phys. Rev. C **29**, 1735 (1984).

[96] J. M. Lattimer and F. D. Swesty, Nucl. Phys. A **535**, 331 (1991).

[97] A. Rios, Nucl. Phys. A **845**, 58 (2010).

[98] O. Lourenço, B. M. Santos, M. Dutra, and A. Delfino, Phys. Rev. C **94**, 045207 (2016).

[99] S. Yang, B. N. Zhang, and B. Y. Sun, Phys. Rev. C **100**, 054314 (2019).